nature communications

Article

https://doi.org/10.1038/s41467-024-51122-1

Sequence-encoded bioactive protein-multiblock polymer conjugates via quantitative one-pot iterative living polymerization

Received: 15 September 2023

Accepted: 30 July 2024

Published online: 07 August 2024

Check for updates

Ziying Li[1], Kaiyuan Song[1], Yu Chen[1], Qijing Huang[1], Lujia You[1], Li Yu[1], Baiyang Chen[1], Zihang Yuan[1,2], Yaqin Xu[1], Yue Su[2], Lintai Da[1] ✉, Xinyuan Zhu[2] & Ruijiao Dong[1] ✉

Protein therapeutics are essential in treating various diseases, but their inherent biological instability and short circulatory half-lives in vivo pose challenges. Herein, a quantitative one-pot iterative living polymerization technique is reported towards precision control over the molecular structure and monomer sequence of protein-polymer conjugates, aiming to maximize physicochemical properties and biological functions of proteins. Using this quantitative one-pot iterative living polymerization technique, we successfully develop a series of sequence-controlled protein-multiblock polymer conjugates, enhancing their biostability, pharmacokinetics, cellular uptake, and in vivo biodistribution. All-atom molecular dynamics simulations are performed to disclose the definite sequence-function relationship of the bioconjugates, further demonstrating their sequence-encoded cellular uptake behavior and in vivo biodistribution in mice. Overall, this work provides a robust approach for creating precision protein-polymer conjugates with defined sequences and advanced functions as a promising candidate in disease treatment.

Proteins form the foundation of the main biological processes essential for life through protein–protein interactions[1,2]. Protein therapeutics have found widespread applications in treating or alleviating various diseases[3–5]. Owing to the inherent biological instability and short half-lives in vivo of pristine proteins[6,7], scientists can enhance their biostability and bioactivity not only by adjusting protein sequences[8,9] and reconfiguring topological structures[10,11], but also by creating protein-polymer conjugates, which has now emerged as a feasible strategy for addressing the aforementioned challenges[12–14]. In this context, two key methodologies including grafting-to and grafting-from are generally adopted to produce protein-polymer conjugates[15,16]. The grafting-to technique directly grafts a presynthesized polymer to the protein, and therefore both the monomer types and polymerization conditions can be customized on-demand. For instance, Perrier[17], Haddleton[18], Francis[19], Lu[20], Johnson[21], and many others[22–24] have done excellent work on the grafting-to synthesis of protein conjugates. However, this grafting-to method generally entails independent synthesis of orthogonal end-functionalized polymers, followed by the covalent conjugation of the presynthesized polymers to proteins. The intrinsic limitations (i.e., steric hindrance, burial of polymer functional end-group, use of organic solvent, etc.) of the covalent grafting of bulky polymers (in particular, hydrophobic ones)

[1]Shanghai Center for Systems Biomedicine, Key Laboratory of Systems Biomedicine (Ministry of Education), Shanghai Jiao Tong University, Shanghai, China. [2]School of Chemistry and Chemical Engineering, Frontiers Science Centre for Transformative Molecules, Shanghai Key Laboratory for Molecular Engineering of Chiral Drugs, Shanghai Jiao Tong University, Shanghai, China. ✉e-mail: darlt@sjtu.edu.cn; drj021@sjtu.edu.cn

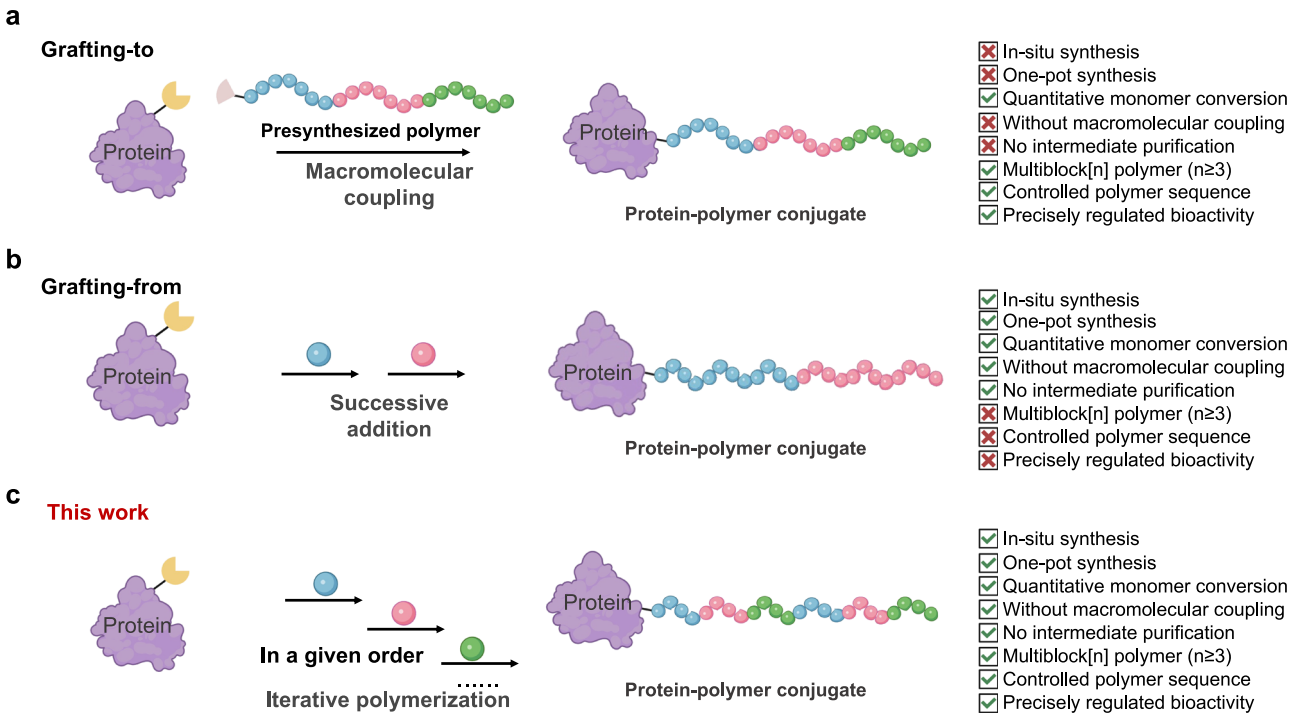

Fig. 1 | Different strategies for producing protein-multiblock polymer conjugates. a Grafting-to method principally relies on the covalent conjugation of the presynthesized polymers to proteins, which cannot achieve one-pot, in-situ synthesis of protein-multiblock polymer conjugates. **b** Grafting-from approach entails tedious multistep synthesis process to fabricate protein-multiblock polymer conjugates, which yet fails to fulfill precision control over the chain structure, monomer sequence and bioactivity. **c** Quantitative one-pot iterative living polymerization enables one-pot, in-situ creation of sequence-controlled protein-multiblock polymer conjugates with controlled monomer sequence and tunable biological functions. Figure 1 Created with BioRender.com released under a Creative Commons Attribution-NonCommercial-NoDerivs 4.0 International license.

to proteins often lead to low protein/polymer coupling efficacy, protein denaturation and complicate purification (Fig. 1a).

In contrast, the grafting-from method refers to in-situ growth of the polymer chains from protein-based macro-initiators or macro-chain transfer agents (macroCTA) via atom transfer radical polymerization (ATRP)[25–27] or reversible addition-fragmentation chain transfer polymerization (RAFT)[28–30], to yield the protein-polymer conjugates. The groups of Lewis[31,32], Russell[33], Gao[34], Sumerlin[35], Velonia[36], Maynard[37], Whittaker[38], and others[39,40] have presented pioneering works on in-situ fabrication of protein conjugates grafting with homopolymers[34,36–40] or diblock copolymers[35] by controlled radical polymerization, and the resultant bioconjugates can be readily isolated via simple dialysis[41,42]. However, this approach yet requires tedious multistep synthesis process towards producing protein-multiblock polymer conjugates accompanied with indispensable intermediate purification, more importantly, the chain structure and monomer sequence of the growing polymer cannot be precisely controlled owing to non-quantitative monomer conversion during each polymerization cycle. Recently, the group of Haddleton[43] has developed a versatile copper-mediated living radical polymerization (Cu-LRP) to synthesize well-defined protein-homopolymer conjugates with full monomer conversion, and Velonia et al.[44] has further reported an oxygen-tolerant copper-mediated polymerization methodology for the ultrafast synthesis of protein-diblock polymer conjugates with quantitative monomer conversion, thereby opening up avenues for the creation of protein-homopolymer or diblock copolymer conjugates in a controlled and quantitative manner (Fig. 1b).

In nature, biomacromolecules possess complicated structures, precisely controlled sequences, and intricate functionalities, and the monomer sequence plays a pivotal role in governing their functional expression[45–48]. Similarly, synthetic polymers with defined monomer sequence and precision monomer unit positioning are of paramount importance in shaping/reconstructing the chain structure and functionality of synthetic polymers for information storage, molecular recognition, and catalysis[49–54]. However, the conventional polymerization approaches fail to achieve high-efficiency, precision control over the chain structure, composition, architecture, molecular weight, and monomer sequence of sophisticated multiblock polymers[48,50,51], greatly limiting their structure optimization, performance improvement, and wide applicability in real life. To the best of our knowledge, the physical and biological advantages of protein-polymer conjugates have rarely been combined with the structural and information-bearing complexity of sequence-controlled multiblock polymers. Therefore, the creation of a facile and robust synthesis methodology for high-efficiency, controlled production of precision protein-multiblock polymer conjugates with well-defined monomer sequence and advanced biological functions is timely and highly challenging.

Herein, we report a robust quantitative one-pot iterative living polymerization (QOILP) strategy that enables precision control over chain structure, molecular weight, monomer sequence, and biological functions, to yield well-defined protein-multiblock polymer conjugates with sequence-encoded bioactivities (Fig. 1c). This QOILP approach holds an advantage towards one-pot, in-situ synthesis of sequence-controlled multiblock polymer bioconjugates without any intermediate purification. To achieve precise control over monomer sequence, three highly-reactive acrylate-based monomers including hydrophobic monomer methyl acrylate (MA, M′), hydrophilic monomer oligo(ethylene glycol) acrylate (OEGA, O′), and monomer containing the functional group 2-hydroxyethyl acrylate (HEA, H′), have been sequentially polymerized in a given order via one-pot iterative ATRP from BSA-Macro with quantitative monomer conversion (>99%) for each cycle (Fig. 2a), to yield six different kinds of sequence-controlled BSA-multiblock polymer conjugates: BSA-(M′$_{20}$-*b*-M′$_{20}$-*b*-M

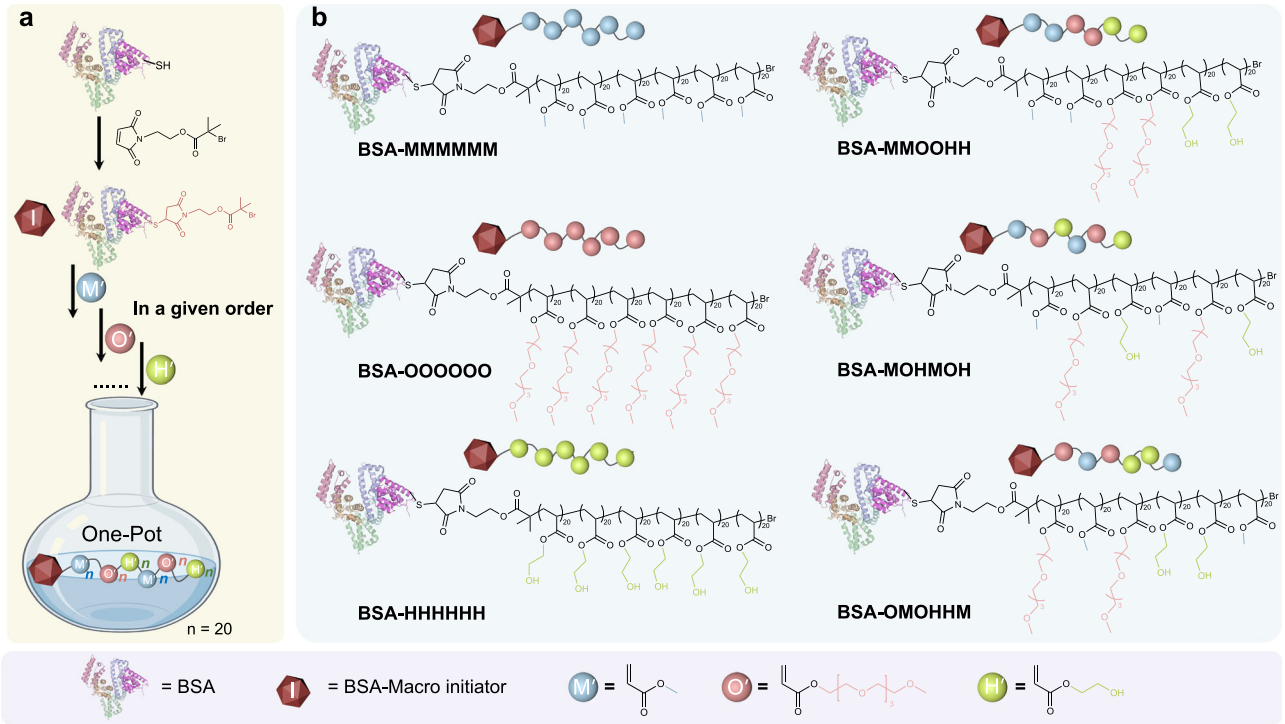

Fig. 2 | Schematic illustration of quantitative one-pot iterative living polymerization. a Quantitative one-pot iterative living polymerization to produce sequence-controlled BSA-multiblock polymer conjugates. **b** Structures of various sequence-controlled BSA-multiblock polymer conjugates synthesized in this work. The capital letters (M, O, and H) stand for approximately 20 acrylate-based monomers MA, OEGA, and HEA, respectively. Figure 2a Created with BioRender.com released under a Creative Commons Attribution-NonCommercial-NoDerivs 4.0 International license.

′$_{20}$-*b*-M′$_{20}$-*b*-M′$_{20}$) (BSA-MMMMMM), BSA-(O′$_{20}$-*b*-O′$_{20}$-*b*-O′$_{20}$-*b*-O′$_{20}$-*b*-O′$_{20}$-*b*-O′$_{20}$) (BSA-OOOOOO), BSA-(H′$_{20}$-*b*-H′$_{20}$-*b*-H′$_{20}$-*b*-H′$_{20}$-*b*-H′$_{20}$-*b*-H′$_{20}$) (BSA-HHHHHH), BSA-(M′$_{20}$-*b*-M′$_{20}$-*b*-O′$_{20}$-*b*-O′$_{20}$-*b*-H′$_{20}$-*b*-H′$_{20}$) (BSA-MMOOHH), BSA-(M′$_{20}$-*b*-O′$_{20}$-*b*-H′$_{20}$-*b*-M′$_{20}$-*b*-O′$_{20}$-*b*-H′$_{20}$) (BSA-MOHMOH), and BSA-(O′$_{20}$-*b*-M′$_{20}$-*b*-O′$_{20}$-*b*-H′$_{20}$-*b*-H′$_{20}$-*b*-M′$_{20}$) (BSA-OMOHHM) (Fig. 2b). This quantitative one-pot iterative polymerization strategy greatly simplifies the synthetic technology without purification of intermediates, but also improves the sequence accuracy, purity and yield of target protein-multiblock polymer conjugates. All-atom molecular dynamics (MD) simulations are used to investigate the structural dynamics of the resultant BSA-multiblock polymer conjugates, further illustrating their interaction modes and architectures in a sequence-dependent manner. Furthermore, sequence-controlled BSA-multiblock polymer conjugates exhibit distinct physicochemical properties and biological functions, in particular, sequence-encoded cellular uptake behaviors, in vivo biodistributions and pharmacokinetics.

Results and discussion

Monomer reactivity screening via model ATRP

One-pot iterative synthesis generally comprises sequential reactions that occur in a single reactor in a preset order without purification of intermediates, providing a high-efficiency platform for fabrication of sequence-controlled polymers. First, the key to one-pot iterative synthesis lies in quantitative monomer conversion during each polymerization cycle. Second, to prevent protein denaturation and maintain the structural intact of proteins during the polymerization process, one-pot iterative living polymerization has to be conducted under mild conditions, i.e., in aqueous medium and at low temperature.

To screen highly reactive monomers that can be efficiently polymerized via ATRP under mild conditions, a readily obtained brominated poly(ethylene glycol) (2 kDa) (PEG$_{2k}$-Br) was chosen as the model macroinitiator to initiate the typical ATRP of a variety of methacrylate- and acrylate-based monomers in an aqueous solution at 35 °C, which allowed real-time monitoring of the polymerization progress by nuclear magnetic resonance (NMR) techniques. The polymerization of methacrylate-based monomers (Supplementary Fig. 21) and acrylamides (*N*,*N*-dimethyl acrylamide and *N*-isopropyl acrylamide) proceeded sluggishly (Supplementary Fig. 22), and never went to completion even after 7 days due to their relatively low rates of propagation (k_p) along with high rates of termination[51]. In contrast, acrylate-based monomers, in particular, the aforementioned MA (M′), OEGA (O′) and HEA (H′), showed quantitative monomer conversion (>99%) as confirmed by ^{1}H NMR spectroscopy with DMF as an internal standard (Fig. 3a and Supplementary Fig. 23), to give well-defined PEG-based diblock copolymers. Therefore, the three reactive acrylates were adopted to produce sequence-controlled protein-multiblock polymer conjugates. In the resulting bioconjugates, the hydrophobic MA block would introduce the hydrophobic interaction with the nonpolar residues on the protein surface, the functional HEA block would enhance the hydrogen-bonding interaction with the polar residues on the protein surface, and the hydrophilic OEGA block could improve the biostability of the protein in vitro or in vivo.

Controlled fabrication of bioactive BSA-multiblock polymer conjugates

The BSA-macroinitiator (BSA-Macro) was site-selectively synthesized via a biorthogonal Michael addition of maleimide-functionalized ATRP initiator to non-bridged cysteine 34 (Cys34) of BSA under milder conditions (in aqueous solution at 7 °C)[55,56], and matrix-assisted laser desorption/ionization time-of-flight mass spectrometry (MALDI–TOF–MS, size exclusion chromatography (SEC) and sodium dodecyl sulfate-polyacrylamide gel electrophoresis (SDS-PAGE) were performed to verify the identity of target BSA-Macro (Fig. 3e, Supplementary Figs. 24 and 38). The monomer conversion ratio of

https://doi.org/10.1038/s41467-024-51122-1

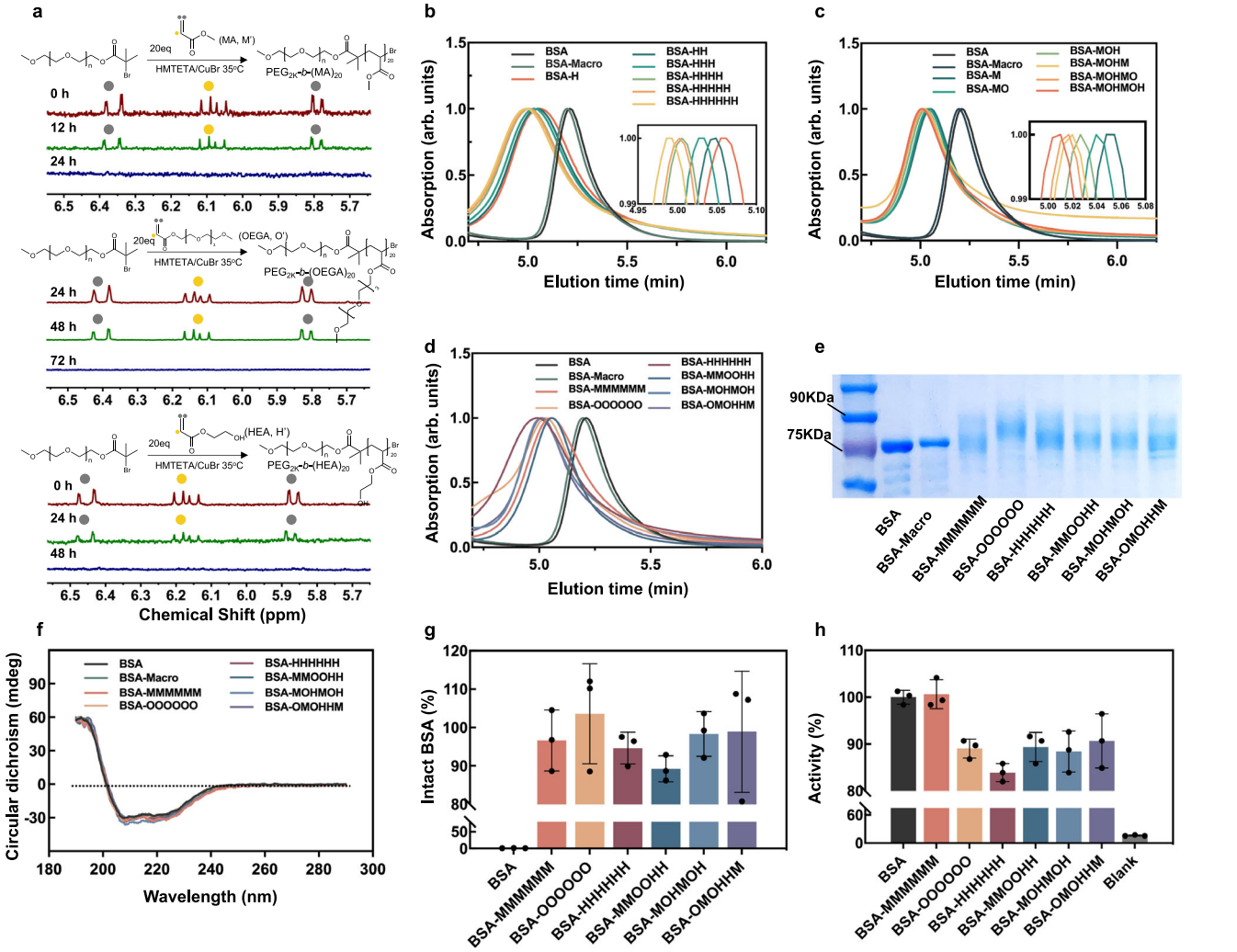

Fig. 3 | Structural characterization of sequence-controlled BSA-multiblock polymer conjugates. a In situ monitoring of ATRP progress of three acrylates (MA, M′; OEGA, O′; HEA, H′) initiated with PEG_{2K}-Br using ^{1}H NMR spectrometry. The quantitative conversion was confirmed with the disappearance of the vinyl signals at 5.8–6.4 ppm. **b**, **c** SEC traces of all growing BSA-multiblock polymer conjugates via QOILP, including (**b**) all bioconjugate intermediates towards BSA-HHHHHH, and (**c**) all bioconjugate intermediates towards BSA-MOHMOH. **d** SEC traces of BSA, BSA-Macro, and six target sequence-controlled BSA-multiblock polymer conjugates. **e** SDS-PAGE of BSA, BSA-Macro, and six target sequence-controlled BSA-multiblock polymer conjugates. Representative images from three independent experiments are shown. **f** CD spectra of BSA and sequence-controlled BSA-multiblock polymer conjugates. **g** Biochemical stability assay of BSA and BSA-multiblock polymer conjugates after heating to 90 °C for 30 min by HPLC ($n = 3$). **h** Esterase-like activities of BSA and BSA-multiblock polymer conjugates. The data are shown as mean ± SD ($n = 3$) for **g** and **h**. Source data are provided as a Source Data file.

three acrylates (MA, OEGA and HEA) via ATRP initiated with BSA-Macro was further analyzed in time by ^{1}H NMR spectroscopy with DMF as an internal standard, and the proton signals at 5.8–6.4 ppm of vinyl groups of all three acrylates finally become undetectable after a certain period of time, demonstrating parallelly quantitative monomer conversion (>99%) (Supplementary Fig. 25).

Then, the freshly prepared BSA-Macro as a macroinitiator was used to initiate the polymerization of MA, OEGA, and HEA, respectively, to produce the BSA-multiblock homopolymer conjugates. SEC was subsequently utilized to examine all growing BSA-multiblock homopolymer conjugates during each polymerization cycle, giving single SEC peaks and further verifying their readily controlled polymerization nature. Along with their chain growth, the SEC retention time of these growing BSA-multiblock homopolymer conjugates gradually shortened, demonstrating a stepwise increase in size and molecular weight (Fig. 3b and Supplementary Fig. 26). After six iterations, three target BSA-multiblock homopolymer conjugates were successfully acquired, including BSA-MMMMMM, BSA-OOOOOO, and BSA-HHHHHH (Supplementary Fig. 27). The structure and molecular weight of the above three bioconjugates were confirmed by ^{1}H NMR spectroscopy (Supplementary Figs. 29–31), SEC (Fig. 3d and Supplementary Fig. 37), SDS-PAGE (Fig. 3e and Supplementary Fig. 38), plus MALDI–TOF–MS (Supplementary Fig. 28 and Supplementary Fig. 35). To verify the controllability of this QOILP strategy, we directly introduced 120 equivalents of acrylates individually at a time in one-pot, and the resultant BSA-polymer conjugates (BSA-120M′, BSA-120O′ and BSA-120H′) exhibited analogous SEC patern, molecular weight and its distribution to those of the aforementioned three BSA-multiblock homopolymer conjugates formed by stepwise addition of 20 equivalents of acrylates for 6 times (Supplementary Fig. 36).

To create sequence-controlled BSA-multiblock copolymer conjugates via QOILP, all three acrylates (MA, OEGA, and HEA) were added in one-pot in a preset sequence and initiated with BSA-Macro under the same condition as above. With each addition of acrylates, the resulting mixture was left for continued polymerization for a certain period of time, ensuring complete monomer conversion (>99%) during each polymerization cycle. All growing BSA-multiblock copolymer conjugates were analyzed by SEC. Likewise, the SEC retention time of the

growing bioconjugate intermediates gradually reduced as the bioconjugates grew in length, verifying a stepwise rise in molecular weight (Fig. 3c and Supplementary Fig. 26). After six iterations, three target sequence-controlled BSA-multiblock copolymer conjugates with defined sequences and specific properties were successfully produced, including BSA-MMOOHH, BSA-MOHMOH, and BSA-OMOHHM, which were further identified by ^{1}H NMR (Supplementary Figs. 29–34), SEC (Fig. 3d and Supplementary Fig. 37), SDS-PAGE (Fig. 3e and Supplementary Fig. 38), and MALDI–TOF–MS (Supplementary Figs. 28 and Supplementary 35). We noted that the appearance of multiple peaks in SEC of all BSA bioconjugates might be attributed to the formation of multimers of BSA (i.e., dimer, trimer, etc.) as well as the resulting clusters of BSA bioconjugates via the interchain entanglement of polymers in solution (Supplementary Fig. 37).

To demonstrate the applicability of this QOILP approach, we further examined and evaluated the polymerization activity of two more protein-based macroinitiators, including GOx-Macro and β-gal-Macro. As depicted in Supplementary Figs. 25 and 26, the quantitative monomer conversion (>99%) of three acrylates (MA, OEGA, and HEA) could be achieved using both GOx-Macro and β-gal-Macro as macroinitiator, validated by in time ^{1}H NMR spectroscopy monitoring (Supplementary Figs. 39a–c and 40a–c), the shortened retention time in SEC (Supplementary Figs. 39d and 40d). ^{1}H NMR spectroscopy (Supplementary Figs. 39e–g and 40e–g), FTIR spectroscopy (Supplementary Figs. 39h and 40 h) and SDS-PAGE (Supplementary Figs. 39i and 40i) further proved the successful formation of bioconjugates, and verified the identity of the resultant GOx-, and β-gal-polymer conjugates (i.e., GOx-M_{50}, GOx-O_{50}, GOx-H_{50}, β-gal-M_{50}, β-gal-O_{50}, and β-gal-H_{50}). We noted that, all GOx bioconjugates show similar activity to the native GOx (Supplementary Fig. 39j), while all β-gal bioconjugates exhibited lower activity than that of the native β-gal (Supplementary Fig. 40j). The results showed that the bioconjugation of GOx had a slight effect on the activity of GOx, and the bioconjugation of β-gal reduced the activity of β-gal to a certain degree. It was noting that the physicochemical properties (i.e., isoelectric point, the secondary structure arrangement, and the surface charge) of proteins (i.e., BSA, GOx, and β-gal) had no effect on the synthesis efficiency of this QOILP approach, demonstrating its universality and wide applicability for the creation of a variety of protein-multiblock polymer conjugates.

Physicochemical properties of BSA-multiblock polymer conjugates

BSA exhibited characteristic circular dichroism (CD) spectra with two negative brands near 209 nm and 220 nm, and a positive peak around 192 nm due to its α-helix structure. In Fig. 3f, BSA-Macro and all six sequence-controlled BSA-multiblock polymer conjugates showed pretty analogical CD bands compared to that of BSA, in particular, a strong positive peak at 191 nm ($\pi \rightarrow \pi^*$) and a characteristic negative doublet at 209 ($\pi \rightarrow \pi^*$) and 220 nm ($n \rightarrow \pi^*$) corresponding to α-helix conformation, indicating that the secondary structure of BSA remained intact during the whole synthesis and polymerization process. Dynamic light scattering (DLS) was carried out to evaluate the hydrodynamic diameters (D_h) of BSA and its bioconjugates in water. The pristine BSA had a hydrodynamic size of ca. 4.46 ± 0.77 nm, while BSA-multiblock polymer conjugates showed increased size in the range of 11.08 ± 0.82 nm to 28.76 ± 1.60 nm (Supplementary Fig. 41 and Supplementary Table 1). The increase in size further confirmed the successful fabrication of BSA-multiblock polymer conjugates. Meanwhile, the sequence alteration of hydrophobic monomer (MA), hydrophilic monomer (OEGA) and hydrogen-bond donor (HEA), had a great effect on the morphologies and aggregated behaviors in solution, eventually leading to a noticeable variation in D_h of the resultant bioconjugates. Both BSA-MMMMMM (17.50 ± 2.91 nm) and BSA-HHHHHH (19.06 ± 0.68 nm) demonstrated relatively larger D_h than that of BSA-OOOOOO (11.08 ± 0.82 nm). All-atom MD simulation verified that BSA-MMMMMM revealed maximum hydrophobic interactions while BSA-HHHHHH had the most intra- or inter-molecular hydrogen bonds compared to BSA-OOOOOO, which further led to the aggregation of BSA-MMMMMM or BSA-HHHHHH in solution to some degree and the subsequent formation of bioconjugate clusters. Compared to BSA-multiblock homopolymer conjugates, the hydrophilicity/hydrophobicity of BSA-multiblock copolymer conjugates could be readily regulated via precisely controlling over the monomer sequence of the grafted copolymer in BSA bioconjugates, in particular, BSA-MMOOHH and BSA-MOHMOH, revealed relatively larger D_h than that of BSA-OMOHHM (Supplementary Table 1).

Indeed, tens of proton-donor residues in BSA, exhibited esterase-like activities towards p-nitrophenyl acetate, to hydrolyze p-nitrophenyl acetate to form acetylated adducts and p-nitrophenol[57]. The esterase-like activity of BSA and BSA-multiblock polymer conjugates were then evaluated by monitoring the hydrolysis of p-nitrophenyl acetate (Fig. 3h and Supplementary Table 2). In Fig. 3h, the resulting BSA bioconjugates had similar yet distinct esterase-like activities towards p-nitrophenyl acetate. The esterase-like activity of these bioconjugates would principally depend on the surrounding environment of the corresponding active residues of BSA (Supplementary Fig. 47). In particular, the conjugated multiblock polymers to BSA might bury the active residues of BSA via hydrogen bonds to inhibit the proton transfer catalysis to different degree. We noted that, all BSA bioconjugates retained more than 80% esterase-like activity of the BSA, noteworthily, BSA-MMMMMM exhibiting nearly 100% esterase activity of BSA, while BSA-HHHHHH having the minimum esterase activity (ca. 83.92 ± 1.93%) of BSA (Supplementary Table 2). All-atom MD simulations demonstrated that BSA-HHHHHH revealed maximum hydrogen bonds in solution (Fig. 4d), which gave rise to the burial of six active catalytic residues of BSA in total (Supplementary Table 3), ultimately leading to a reduction in esterase-like activity. In contrast, BSA-MMMMMM had no hydrogen bonding with BSA (Fig. 4d), in this case, the active catalytic residues of BSA would almost stay undisturbed, further resulting in a much higher catalytic activity retention.

The thermostability of sequence-controlled BSA-multiblock polymer conjugates was examined by SEC using an accelerated heating test[37]. After being heated up to 90 °C for 30 min, the resultant BSA-multiblock polymer bioconjugates yet held much higher intact BSA content (>90%) compared to the pristine BSA (Fig. 3g, Supplementary Fig. 42, and Supplementary Tables 4 and 5). All-atom MD simulation verified that the grafted multiblock polymers would interact with BSA via hydrophobic interaction and/or hydrogen bonds to some degree (Fig. 4d, e), thereby inducing the burial of BSA surface to different degree (Fig. 4b). In this case, the partial burial of BSA would definitely protect the BSA from thermal degradation, greatly improving the thermostability of BSA bioconjugates. We further performed variable temperature circular dichroism (VT-CD) to investigate the thermal stability of BSA and its bioconjugates (Supplementary Fig. 43). The variable temperature CD spectra ranging from 25 °C to 95 °C were acquired (Supplementary Fig. 43a–g), and the melting temperature (T_m) of BSA and BSA-polymer conjugates was subsequently calculated by analyzing the peak intensity at 209 nm using sigmoid function (Supplementary Fig. 43h). In Supplementary Table 4, all BSA bioconjugates held much higher T_m (>81 °C) than that of BSA itself (70.81 °C), which was consistent with the results in Fig. 3g and Supplementary Table 6, demonstrating that the conjugation of multiblock polymers to BSA greatly improved the thermal stability of the resulting BSA bioconjugates.

Structural dynamics of BSA-multiblock polymer conjugates

All-atom MD simulations was further performed to investigate the structural dynamics of the aforementioned BSA-multiblock polymer conjugates (Fig. 4a). In each model of these six BSA-multiblock polymer conjugates, the grafted multiblock polymer chain maintained an

https://doi.org/10.1038/s41467-024-51122-1

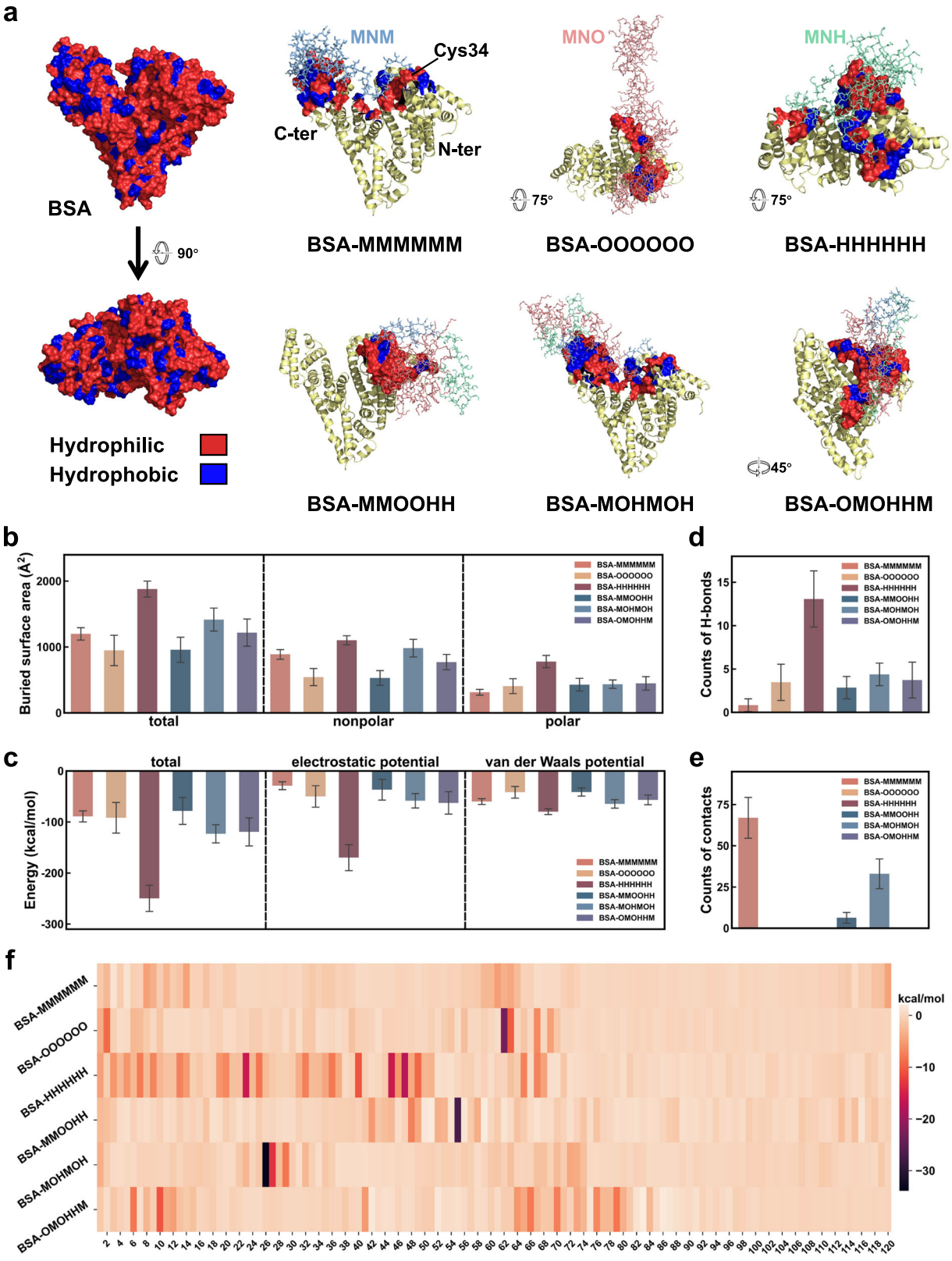

extended conformation using the PACKMOL[58] package at the beginning and a 500-ns MD simulation was then conducted based on the initial model for each system (Supplementary Fig. 44). The results showed that the multiblock polymer chain in each system could be quickly contracted and aggregated onto the BSA surface, and ultimately reached equilibrium after around 300 ns (Supplementary Fig. 45a). The extension of the simulation time up to 1 μs for BSA-MMMMMM did not lead to any significant structural rearrangement, suggesting that a 500-ns MD sampling was fairly sufficient (Supplementary Fig. 45b, d). Additionally, the site-selective conjugation of a multiblock polymer chain imposed no profound structural perturbation on BSA (Supplementary Fig. 45c). The last 200-ns MD dataset was adopted for final structural analyses in each system (see Supplementary information).

Fig. 4 | Sequence-dependent protein/polymer interactions elucidated by all-atom MD simulations. a The last-frame MD snapshots of six BSA-multiblock polymer conjugates with different monomer sequences. The multiblock polymer is shown by sticks and colored by monomer type (pale blue for monomer M′ or MNM, pale red for monomer O′ or MNO, and pale green for monomer H′ or MNH). The interaction residues of BSA with the multiblock polymer are represented on the surface and colored according to their hydrophobic nature (blue) or hydrophilic nature (red). The interaction residues are determined using a distance cut-off of 6 Å, and the overall surface representation of BSA is shown on the left. **b** Buried surface area of BSA in each conjugate system calculated for all residues (left), polar residues (middle), and nonpolar residues (right). **c** The total interaction energies between BSA and the multiblock polymer for each conjugate system (left), and the contributions of the electrostatic and van der Waals interactions are shown in the middle and right panels. The error bars in **b** and **c** show the average values over the last 200-ns MD simulations, with the corresponding standard deviations. **d** Counts of hydrogen-bonds between BSA and the multiblock polymer. **e** Counts of hydrophobic contacts between BSA residues and the methyl group of monomer M′. The counts of contacts were calculated only for the heavy atoms, with a distance cut-off of 4.5 Å. **f** Decomposition of the interaction energy according to each monomeric unit in distinct BSA-multiblock polymer conjugate systems. The data in **b**–**f** show average values over 200 frames with an interval of 1 ns from the last 200-ns MD simulations. The error bars in **b**–**e** show standard deviations. Source data are provided as a Source Data file.

According to the MD results, distinct monomer sequences for these BSA-multiblock polymer conjugates could indeed alter protein/polymer interactions, thereby affecting their binding interfaces. To explore the stability of each BSA-multiblock polymer conjugate, we calculated the buried surface area of BSA upon multipolymer binding and the interaction energies between BSA and multiblock polymer (i.e., electrostatic and van der Waals interactions) by the gmx_MMPBSA[59] package. Among the six bioconjugates, BSA-HHHHHH demonstrated the largest buried surface area (~1900 Å^2) and the lowest interaction energy (ca. −250 kcal/mol) (Fig. 4b, c), indicating more favorable protein/multiblock polymer contacts compared with other bioconjugates. Further hydrogen-bond analyses verified that BSA-HHHHHH established the most hydrogen-bonds with BSA (Fig. 4d), conferred largely by the hydroxyl group of HEA monomer (H′). Although BSA-MMMMMM and BSA-OOOOOO displayed comparable buried surface area and interaction energies, the latter contained more favorable hydrogen-bond interactions (Fig. 4d) between BSA and hydrophilic multiblock polymer chain. For BSA-MMMMMM, nonpolar contacts were proven to be more critical interactions. Importantly, precise alteration or control over monomer sequence could further finely regulate the protein/polymer interactions. In particular, BSA-MOHMOH and BSA-OMOHHM show more favorable protein/polymer interactions compared with BSA-MMMMMM and BSA-OOOOOO (Fig. 4c). Also, the methyl group of MA monomer (M′) in BSA-MOHMOH exhibited more hydrophobic contacts with BSA surface compared to BSA-MMOOHH and BSA-OMOHHM (Fig. 4e).

We further delineated the energy contribution of each monomeric unit along these sequence-controlled multiblock polymer chains, and thereby these six bioconjugates revealed distinct interaction patterns with varied hot-spot binding sites (Fig. 4f). In accordance with the interaction-energy analyses, BSA-HHHHHH exhibited more hot-spot binding sites where a number of hydrogen-bond networks could be formed between BSA and the multiblock polymer via the hydroxyl group in HEA monomer (H′) (Fig. 4f and Supplementary Fig. 46). For BSA-MMMMMM, nonpolar contacts were dominant in protein/polymer interactions, e.g., the MNM61 unit could be inserted into a shallow hydrophobic pocket formed by T507, F508, H509, E564, F567, and A568. For BSA-OOOOOO, the OEG side-chain oxygen atoms in OEGA monomer (O′) could be trapped by positively-charged lysine residue such as BSA-K127 that participated in stabilizing MNO62 and MNO63 (Supplementary Fig. 46). Intriguingly, the above lysine-oxygen interactions were also observed in other BSA-multiblock polymer systems, for example, MNO55 in BSA-MMOOHH, MNO26–27 in BSA-MOHMOH, and MNO10 in BSA-OMOHHM (Supplementary Fig. 46). In addition, diverse hydrogen-bond forms could also be found in BSA-OMOHHM (e.g., via E470, G85, and T83). In addition, the local conformations of active pockets of BSA (i.e., Sudlow sites 1 and 2) were not disturbed (Supplementary Fig. 48a-c), since none of grafted multiblock polymers reached the active pockets of BSA. Furthermore, it was noting that, for the noncovalent BSA/polymer assembly without the covalent linkage, the buried surface area and hydrogen bonds were drastically reduced (Supplementary Fig. 49a–c), indicating that both the covalent linkage and monomer sequence played a key role in the protein/polymer interplay. These results demonstrated, at the atomic level, the specific hot-spot binding sites in both BSA and the multiblock polymers were responsible for regulating the physicochemical properties and biological activities of protein-multiblock polymer conjugates.

Sequence-dependent cellular uptake

The biocompatibility of BSA and BSA-multiblock polymer conjugates was evaluated using MTT assay. In fact, all BSA-multiblock polymer conjugates exhibited much lower cytotoxicity against both L929 and NIH-3T3 cell lines. In Fig. 5b and Supplementary Fig. 50, the cell viability for all BSA bioconjugates almost remained 100% at the concentration of 250 μg/mL or less. Even if the concentration was increased up to 500 μg/mL, the cell viability of BSA bioconjugates was still higher than 90%, indicating the excellent biocompatibility of the resultant BSA-multiblock polymer conjugates. These results demonstrated that the QOILP offered a facile and efficient approach for the fabrication of protein-multiblock polymer conjugates with well-defined structures and sequences, as well as optimal physiochemical and biological properties. The sequence-dependent cellular uptake behaviors (Fig. 5a) of various sequence-controlled BSA-multiblock polymer conjugates with varied sequences in L929 cell lines were investigated by flow cytometry and confocal laser scanning microscopy (CLSM). BSA and BSA-multiblock polymer conjugates were firstly labeled with the NIR dye Cy5.5 enabling real-time monitoring and imaging in vitro, and L929 cells were then incubated with Cy5.5-labeled BSA or its bioconjugates for a range of times up to 4 h. As shown in Fig. 5e, well-distributed fluorescence signal was clearly observed from L929 cells incubated with the BSA-multiblock polymer conjugates at the early stage (0.5 h), whereas negligible fluorescence could be detected from L929 cells incubated with BSA. This result demonstrated that sequence-controlled multiblock polymers greatly facilitated cellular uptake of the resultant bioconjugates by L929 cells. With the extension of incubation time, intracellular fluorescence intensity of L929 cells incubated with BSA or BSA-multiblock polymer conjugates gradually increased, which was confirmed by flow cytometry and CLSM (Fig. 5c and Supplementary Fig. 51), further demonstrating that both BSA and BSA-multiblock polymer conjugates were taken up by cells in a time-dependent manner.

The effect of monomer sequence of the multiblock polymer on cellular uptake behaviors of BSA-multiblock polymer conjugates was further investigated (Fig. 5c, d and Supplementary Fig. 52). After 0.5 h incubation, the fluorescence intensities of L929 cells incubated with three BSA-multiblock copolymer conjugates (i.e., BSA-MMOOHH, BSA-MOHMOH, and BSA-OMOHHM), were higher than the other three BSA-multiblock homopolymer conjugates (i.e., BSA-MMMMMM, BSA-OOOOOO, and BSA-HHHHHH), in particular, BSA-OMOHHM revealed the fastest cell penetration rate, roughly 2- to 3-fold higher than that of these multiblock homopolymer conjugate systems (Fig. 5c). The variation in cell penetration rate of the bioconjugates might be tentatively attributed to distinct buried surface areas of BSA in each system

https://doi.org/10.1038/s41467-024-51122-1

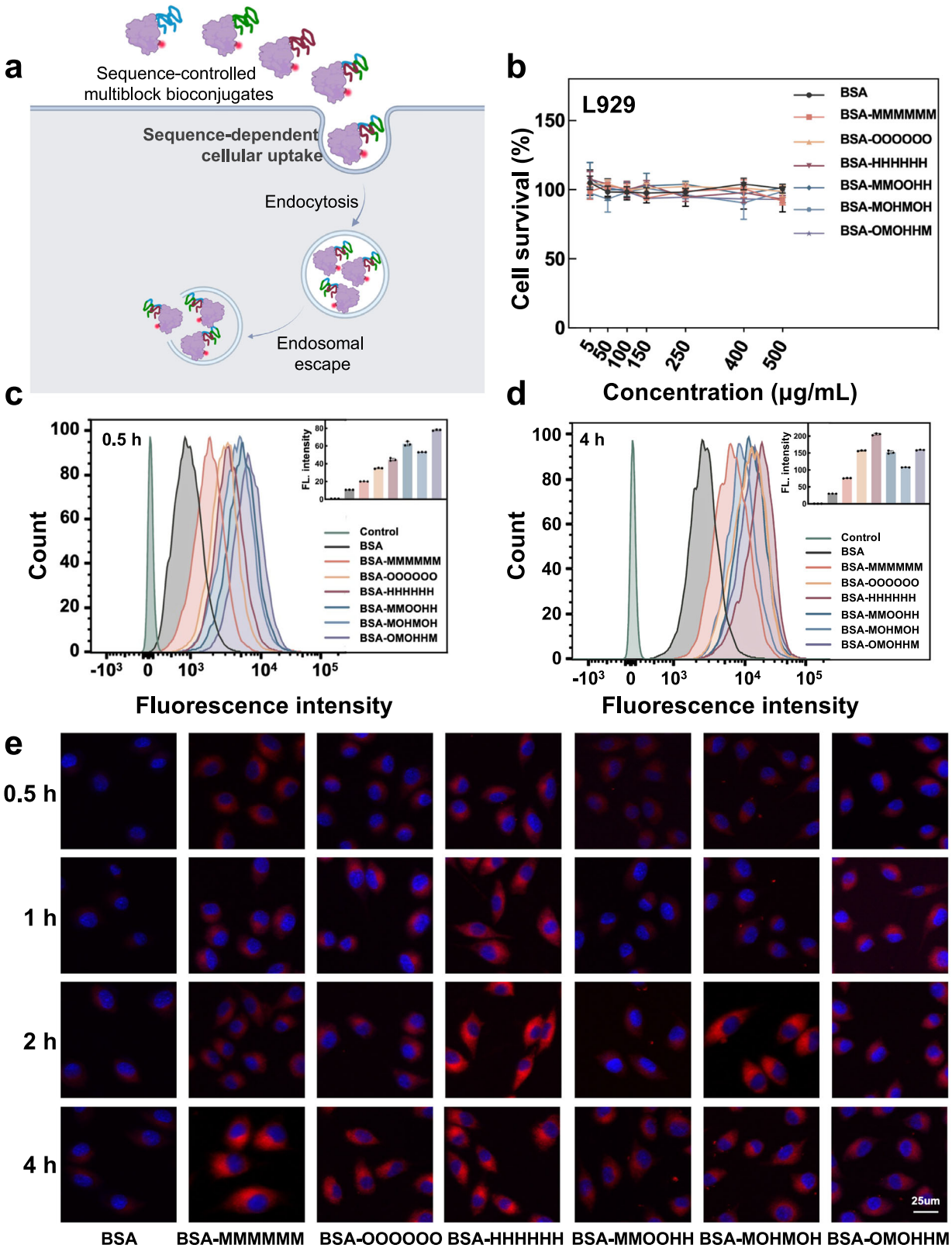

Fig. 5 | The in vitro cytotoxicity and cellular uptake of BSA-multiblock polymer conjugates by L929 cells. a The illustration of the sequence-dependent cellular-uptake process. **b** Cytotoxicity assay of BSA and sequence-controlled BSA-multiblock polymer conjugates incubated with L929 cells for 24 h. **c**, **d** Cellular uptake of Cy5.5-labeled BSA and Cy5.5-labeled BSA-multiblock polymer conjugates by L929 cells detected by flow cytometry for (**c**) 30 min and (**d**) 4 h. Insert: Quantitative fluorescence (FL) intensity comparisons based on the fluorescence-activated cell sorting (FACS). **e** Confocal images of L929 cells after incubation with Cy5.5-labeled BSA and Cy5.5-labeled BSA-multiblock polymer conjugates for different times (blue: DAPI, red: Cy5.5). Representative images from three independent experiments are shown. The data are shown as mean ± SD ($n = 4$) for **b** and the data are shown as mean ± SD ($n = 3$) for **c** and **d**. Figure 5a Created with BioRender.com released under a Creative Commons Attribution-NonCommercial-NoDerivs 4.0 International license. Source data are provided as a Source Data file.

determined by MD simulations as above (Fig. 4b). After 4 h incubation, L929 cells incubated with BSA-HHHHHH had the strongest fluorescence (Fig. 5c, e), demonstrating highest cell internalization efficiency. It could be attributed to the fact that BSA-HHHHHH showed the maximum hydrogen bonds and the largest buried surface area according to all-atom MD simulations (Fig. 4b, d), which effectively shielded the negative charge of BSA, further facilitating the cellular uptake of the resulting bioconjugate by L929 cells. With alteration in monomer sequence, the fluorescence intensity of BSA-multiblock polymer conjugates increased to varying degrees, disclosing specific sequence-encoded cellular internalization behaviors as depicted in Fig. 5a. Thus, the precision control over the monomer sequence of BSA-multiblock polymer conjugates paved an avenue towards high-efficiency regulation and improvement of the cellular penetration behaviors.

Sequence-encoded in vivo biodistribution and pharmacokinetic

To further evaluate the effect of monomer sequence on in vivo biodistribution of various sequence-controlled BSA-multiblock polymer conjugates, in vivo near-infrared (NIR) fluorescence imaging was performed in BALB/c mice. After an intravenous injection of Cy5.5-labeled BSA and Cy5.5-labeled BSA-multiblock polymer conjugates, the NIR fluorescence images of BALB/c mice were acquired at predetermined time points (Fig. 6a). At 0.5 h post-injection, the NIR fluorescence was detected throughout the body, and the fluorescence intensity of all BSA-multiblock polymer conjugates in BALB/c mice decayed with time. In vivo biodistribution of BSA and BSA-multiblock polymer conjugates was further investigated by qualitative or quantitative analysis of the fluorescence of excised organs (Fig. 6b, c). The major organs (heart, liver, spleen, lungs, and kidneys) were then harvested after the mice being killed at different injection time intervals. Images of major organs harvested 1 h, 4 h, and 8 h post-injection are depicted in Fig. 6c and Supplementary Fig. 53. The pristine BSA showed much lower mean fluorescence intensity in all organs, suggesting shorter circulatory half-life in vivo ascribed to its biological instability and fast clearance. In contrast, all BSA-multiblock polymer conjugates underwent slower renal clearance and accumulated in liver, kidneys, lung, and spleen. The results indicated that the site-specific conjugation of multiblock polymers to proteins could effectively prolong their circulation time in vivo.

Apparently, these BSA-multiblock polymer conjugates with different monomer sequences displayed distinct levels of enrichment in various organs (Fig. 6c). To accurately visualize the biodistribution of sequence-controlled BSA-multiblock polymer conjugates in various organs of BALB/c mice, we quantified the fluorescence intensity of major organs at different time intervals. In Fig. 6b, the fluorescence intensity declined to varying degrees in various organs as time progressed. In the heart, there was no significant difference in fluorescence intensity among each bioconjugate after 1 h injection, noteworthily, BSA-MMOOHH remained highly enriched over time. Initially, BSA-OOOOOO showed higher enrichment in the liver, while BSA-HHHHHH maintained its enrichment in the liver as time passed. In the spleen, all six BSA-multiblock polymer conjugates showed good enrichment, and all bioconjugates except BSA-MOHMOH experienced attenuation over time. At the early stage of injection, three BSA-multiblock copolymer conjugates had greater fluorescence intensity in the lung than that of BSA-multiblock homopolymer conjugates, but the former decayed more quickly over time than the latter. The three BSA-multiblock copolymer conjugates (i.e., BSA-MMOOHH, BSA-MOHMOH, and BSA-OMOHHM) were less enriched in the kidney than BSA-multiblock homopolymer conjugates, revealing that protein conjugation with sequence-controlled multiblock copolymers could reduce the renal clearance of therapeutic proteins to a great extent. Therefore, it could be concluded that the precision control over monomer sequence could finely regulate protein/polymer interactions in bioconjugates (Fig. 4), further optimizing their biodistribution in vivo.

In vivo pharmacokinetics studies of BSA-multiblock polymer conjugates were then conducted by intravenous injection of BSA and BSA-multiblock polymer conjugates in Sprague-Dawley (SD) rats. Figure 6d showed the concentration of BSA and BSA-multiblock polymer conjugates in the plasma over time after injection, and the pharmacokinetic parameters of BSA and its bioconjugates were calculated by fitting the two-compartment model as summarized in Supplementary Table 7. It's worth noting that all samples were rapidly distributed in SD rat tissues post-injection. Compared to the pristine BSA, the plasma BSA levels of BSA-multiblock polymer conjugates declined slowly over time, as indicated by the longer distribution half-life ($t_{1/2,\alpha}$). Followed by a rapid distribution phase, BSA and its bioconjugates underwent a slower elimination phase. All BSA-multiblock polymer conjugates had a longer elimination half-life at the beta phase ($t_{1/2,\beta}$) than BSA, demonstrating a greatly improved pharmacokinetic profile. Among the BSA-multiblock homopolymer conjugates, BSA-MMMMMM showed a longer terminal half-life ($t_{1/2,\beta}$) compared to BSA-OOOOOO and BSA-HHHHHH. In particular, BSA-OMOHHM showed the longest terminal half-life time ($t_{1/2,\beta}$) of 18.53 h among all BSA-multiblock polymer conjugates. The difference in pharmacokinetics of BSA-multiblock polymer conjugates might be mainly attributed to their sequence-encoded interaction patterns, morphologies, and bioactivities in vivo.

We have illustrated that a facile and robust QOILP synthetic strategy can be successfully applied to the production of sequence-controlled protein-multiblock polymer conjugates with precisely controlled monomer sequence and readily tunable biological functionalities. This quantitative QOILP approach not only simplifies the synthetic technology without isolation of intermediates between each polymerization cycle, but also improves the sequence accuracy, purity, and yield of target protein-multiblock polymer conjugates. All-atom MD simulations were utilized to elucidate the structural dynamics of sequence-controlled protein-multiblock polymer conjugates, further unveiling their sequence-dependent interaction modes and architectures. The precision control over monomer sequence at the molecular level led to a significant enhancement in biostability, esterase-like activity, and biocompatibility of the resultant protein bioconjugates. In vitro and in vivo studies further verified that BSA-multiblock polymer conjugates were endowed with sequence-encoded cellular uptake behaviors, finely regulated in vivo biodistribution, and improved in vivo pharmacokinetics to varying degree. We believe that the QOILP strategy will pave the way to the creation of molecularly-precise, multidimensionally-ordered protein-polymer conjugates with defined monomer sequence, controlled hierarchical structures and tunable functionalities, further enabling the development of next-generation protein therapeutics with maximized therapeutic efficacy as a splendid candidate in disease treatment.

Methods

Ethical statement

All animal experiments were carried out in compliance with the 3R principle, and were approved by the Institution Animal Care and Use Committee of Shanghai Jiao Tong University under approval number of O A2023010.

Synthesis of BSA-Macro[55,56]

To the solution of BSA (1 equiv.) in 20 mM phosphate buffer (pH 7.4) was slowly added a solution of 2-(2,5-dioxo-2,5-dihydro-1H-pyrrol-1-yl) ethyl 2-bromo-2-methylpropanoate in DMSO (126 mM, 0.8 mL). The reaction mixture was gently shaken for 48 h at 7 °C. The resultant mixture was subsequently dialyzed initially against 10% DMSO in 5 mM phosphate buffer (pH 7.4) and then twice against 20 mM phosphate buffer (pH 7.4) using regenerated cellulose dialysis membranes with a MWCO of 10 kDa. The target product was obtained after lyophilized to remove the solvent and then stored at −20 °C.

https://doi.org/10.1038/s41467-024-51122-1

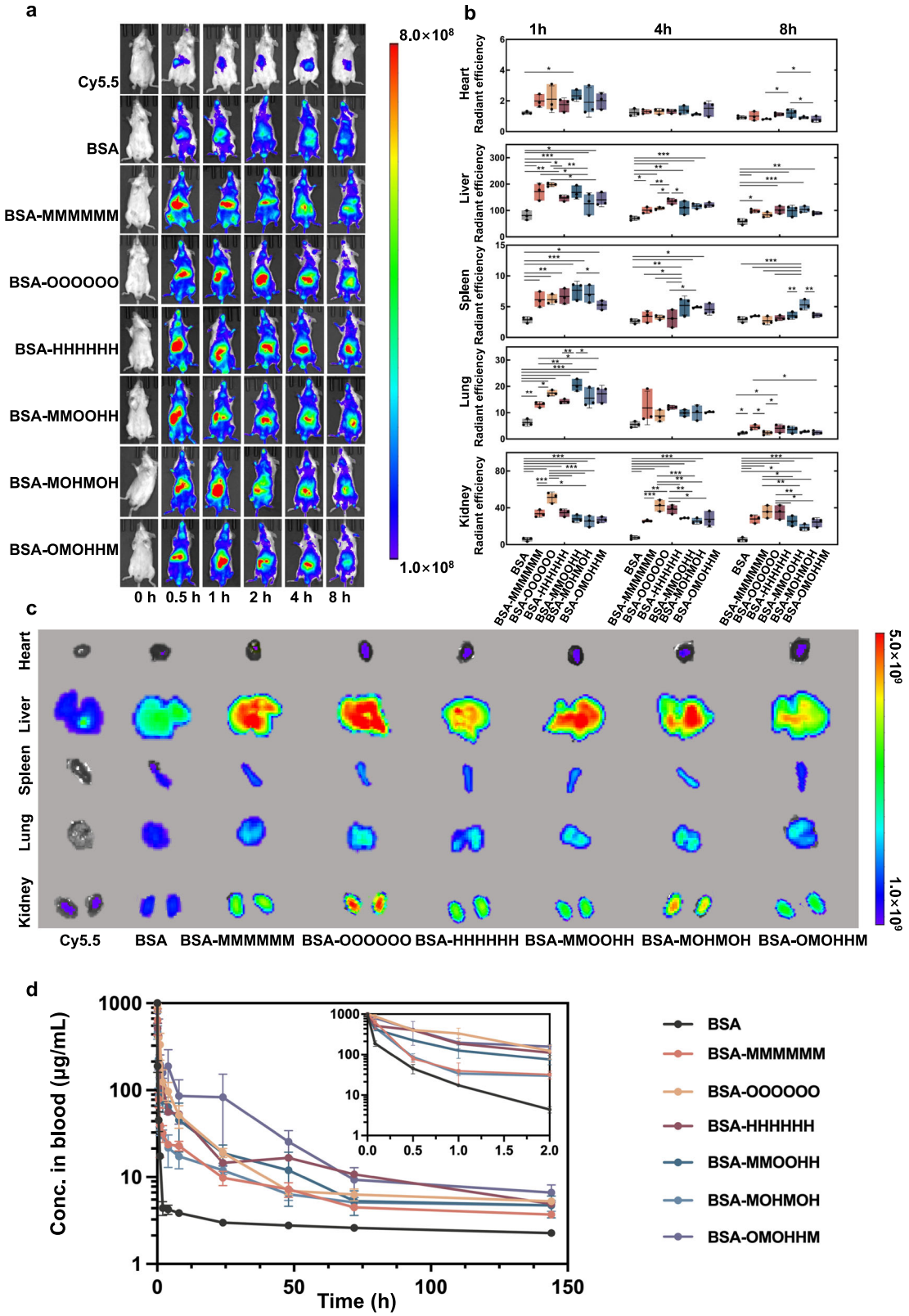

Fig. 6 | In vivo biodistribution and pharmacokinetic of BSA-multiblock polymer conjugates in BALB/c mice. a In vivo fluorescence images of BALB/c mice at different time intervals after intravenous injection of Cy5.5, Cy5.5-labeled BSA, and Cy5.5-labeled BSA-multiblock polymer conjugates, respectively. **b** Quantitation analysis of fluorescence intensity in major organs after injection of Cy5.5-labeled BSA and Cy5.5-labeled BSA-multiblock polymer conjugates for 1 h, 4 h, and 8 h. The data are shown as mean ± SD ($n = 3$). Statistical significance was assessed using a one-way ANOVA with Fisher's LSD test (*$p < 0.05$, **$p < 0.01$, and ***$p < 0.001$). The exact p values are provided in Source Data file. **c** Ex vivo images of excised tissues after injection of Cy5.5-labeled BSA and Cy5.5-labeled BSA-multiblock polymer conjugates. **d** Plasma concentrations of BSA and BSA-multiblock polymer conjugates versus time. The data are shown as mean ± SD ($n = 3$) for **b** and **d**. Source data are provided as a Source Data file.

General procedure for synthesizing BSA-multiblock polymer conjugates

To synthesize BSA-multiblock polymer conjugates, BSA-Macro and the first acrylate were added into an aqueous solution containing 5% DMF. The mixture was then bubbled with N_2 for 30 min. Then, HMTETA and Cu(I)Br was successively added to the mixture. The molar ratio of [BSA-Macro]:[CuBr]:[HMTETA] was set as 1:40:80. The second aliquot of acrylate was supplemented after 3 days. The number of acrylates for each block was 20 equivalents. After six iterations, the reaction mixture was exposed to air and dialyzed initially against 10% DMSO in 5 mM phosphate buffer (pH 7.4) and then twice against 20 mM phosphate buffer (pH 7.4) using regenerated cellulose dialysis membranes with a MWCO of 10 kDa. The target product was obtained after lyophilized to remove the solvent and then stored at −20 °C.

Cy5.5-labeled BSA-multiblock polymer conjugates

The labeling experiment was performed by adding 50 μL (about 5-fold molar excess) Cy5.5 stock solution in DMF (1 mg/mL) to 1 mL BSA-multiblock polymer conjugate solution (1 mg/mL, 10 mM PBS buffer, pH 7.4). The resultant mixture was incubated overnight at room temperature in the dark. Then, excess Cy5.5 were removed by dialysis to yield Cy5.5-labeled BSA-multiblock polymer conjugates.

Nuclear magnetic resonance

^{1}H NMR spectra were recorded at 400 MHz on a Bruker AVANCE III HD 400 NMR spectrometer. NMR spectra were measured at 298 K in $CDCl_3$ or D_2O. Their proton residuals are used as internal reference for ^{1}H NMR, respectively. Proton chemical shifts (δ) are reported in ppm and coupling constants (J) in Hertz (Hz). The multiplicity in the ^{1}H NMR spectra are described as s (singlet), d (doublet), dd (doublet of doublets), t (triplet), q (quartet), m (multiplet), br (broad).

Matrix-assisted laser desorption/ionization time of flight mass spectrometry

MALDI-TOF-MS in positive linear mode was used. The MALDI-7090™ TOF/TOF MS instrument was equipped with a solid-state ultrafast UV laser (Nd: YAG 355 nm). Protein samples were mixed with matrix (1:1 volume ratio, sinapinic acid, 10 μM) and air-dried before analysis, and the resulting mixtures were spotted onto a MALDI plate. The samples were air-dried, then run in linear modes.

Size exclusion chromatography

SEC analysis was performed on an Agilent GPC system was equipped with an Xbridge Protein BEH SEC column (size: 2.1 × 150 mm, 1.7 μm). PBS buffer (50 mM Na_2HPO_4, 50 mM $Na_2HPO_4{\cdot}H_2O$) was used as an eluent at a flow rate of 0.25 mL/min at 30 °C.

Circular dichroism

CD was performed with a JASCO J-1500 spectrometer. CD spectra of BSA and its bioconjugates were recorded in 1 mm quartz cuvettes at 25 °C between 190 nm and 290 nm. The concentration of samples was 0.1 mg/mL in 10 mM phosphate buffer (pH 7.4).

Dynamic light scattering

DLS measurements were carried out using Malvern Zetasizer Nano-zs90. Samples were prepared at the concentration of 1 mg/mL (protein). The instrument was operated at a laser wavelength of 633 nm and a scattering angle of 90° at 25 °C. All results were analyzed with Zetasizer software 6.32.

Sodium dodecyl sulfate-polyacrylamide gel electrophoresis

The samples were dissolved in SDS-PAGE loading buffer containing 5% (v/v) 2-mercaptoethanol and 0.5% (m/v) bromophenol blue. After being heated at 95 °C for 5 min, the samples were loaded onto a pre-cast 10% polyacrylamide gel (5% stacking gel and 10% separation gel). The gel was run on a Protein Gel Apparatus (Bio-Rad) at 80-120 V for 100 min in running buffer (25 mM Tris, 250 mM glycine, and 0.1% SDS), followed by Coomassie Blue staining.

Bicinchoninic acid assay

The protein contents of the samples were determined by using a protein BCA assay kit (Beyotime) following the manufacturer's instructions, and bovine serum albumin was used as the protein standard.

Inductively coupled plasma optical emission spectrometry

Copper contents in BSA-multiblock polymer conjugates (0.5 mg BSA-equivalent/mL in PBS) were analyzed by inductively coupled plasma optical emission spectrometry (PerkinElmer NexION2000G). RF power was 1.6 kW, and flow rate of cooling gas, atomizer gas8 and auxiliary gas were 15 L/min, 1.02 L/min, and 1.2 L/min, respectively. The copper concentrations in all six BSA-multiblock polymer conjugates, including BSA-MMMMMM, BSA-OOOOOO, BSA-HHHHHH, BSA-MMOOHH, BSA-MOHMOH, and BSA-OMOHHM, were determined to be 1.14 ppm, 0.73 ppm, 0.74 ppm, 1.59 ppm, 2.04 ppm, and 1.18 ppm, respectively. The trace amounts of copper were negligible, and they would not be toxic toward the organisms.

Infrared spectroscopy

Infrared spectroscopy was performed with a Nicolet iN10 MX Micro Attenuated Total Reflection Fourier Transform Infraed spectrometer using Omnic (Thermo Electron Corporation) software.

Esterase-like activity measurement[57]

190 μL of BSA, BSA-Macro or BSA-multiblock polymer conjugates containing 0.1 mg/mL of BSA in PBS (10 mM) was loaded into wells of a 96-well plate, and then 10 μL of p-nitrophenyl acetate (PNPA) (10 mM) in PBS containing 20% (v/v) acetonitrile was added into each well. After incubation at room temperature for 30 min, the absorbance of the solution at 405 nm was measured for each sample to evaluate the bioactivities. Each sample was tested in triplicate. The concentration of protein was measured by Bicinchoninic acid (BCA) assay.

Stability study[37]

The freshly prepared solutions of BSA and BSA-multiblock polymer conjugates (0.5 mg/mL) were aliquoted 1000 μL into 1.5 mL centrifuge tubes and heated in a dry heat block at 90 °C for 30 min. The samples with or without heating were analyzed by SEC. The total area under the curve was used to determine the amount of intact BSA.

Cytotoxicity of BSA and BSA-multiblock polymer conjugates

L929 and NIH-3T3 cell lines were obtained from the Cell Bank of Chinese Academy of Science (Shanghai, China). L929 and NIH-3T3 cell lines were cultured in DMEM high glucose medium containing 10% (v/v) fetal bovine serum (FBS) and 1% penicillin/streptomycin (Hyclone) at 37 °C in a humidified, 5% CO_2 atmosphere. For bioassays, the cells were firstly seeded in a 96-well plate (Corning) (50 μL, 5000 cells per well) for attachment overnight, and then serial dilutions (5, 50, 100, 150, 250, 400, 500 μg/mL) of the samples prepared in culture media were added to the test wells (100 μL to each well in tuplicate). Wells filled with media and media-treated cells only were used as background and control, defined as 0% and 100% cell viability, respectively. After 24 h incubation, the survival rate of cells was determined by MTT assay according to MTT kit (Beyotime). The data were analyzed by GraphPad Prism 9.0 software and presented as mean ± standard deviation.

FACS analysis of BSA and BSA-multiblock polymer conjugates

L929 cells were cultured in DMEM high glucose medium containing 10% (v/v) fetal bovine serum (FBS) and 1% penicillin/streptomycin (Hyclone) at 37 °C in a humidified, 5% CO_2 atmosphere. L929 cells were

seeded in a 6-well plate at a density of 200000 cells per well and incubated overnight, the attached cells were next incubated with 5 μM Cy5.5 equivalent of BSA and BSA-multiblock polymer conjugates at 37 °C for 0.5 h, 1 h, 2 h, 4 h. After that, the cells were washed with PBS (Gibco) for three times, and the cells (10000 cells/mL, 0.5 mL) were harvested for FACS analysis.

Intracellular delivery of BSA and BSA-multiblock polymer conjugates

L929 cells were cultured in DMEM high glucose medium containing 10% (v/v) fetal bovine serum (FBS) and 1% penicillin/streptomycin (Hyclone) at 37 °C in a humidified, 5% CO_2 atmosphere. L929 cells were seeded at 50000 per dish in 35 mm glass bottom culture dish (NEST) overnight for attachment. The attached cells were next incubated with 5 μM Cy5.5 equivalent of BSA and BSA-multiblock polymer conjugates at 37 °C for 0.5 h, 1 h, 2 h, 4 h. After that, the cells were washed with PBS (Gibco) and fixed with 4 % (w/v) cold paraformaldehyde for 15 min. Then, the cell nucleus was stained with 2.5 μg/mL DAPI (Sigma) for 10 min. After washed with PBS for three times, the cells could be imaged with Leica TCS SP8 laser scanning confocal microscope. The excitation and emission wavelengths of DAPI, and Cy5.5 were 360/460 nm, and 673/707 nm, respectively. Images were analyzed by LAS X software.

Pharmacokinetics of BSA and BSA-multiblock polymer conjugates

BALB/c mice and SD rats were purchased from the Shanghai Jiao Tong University Laboratory Animal Center. Male mice aged 6 to 8 weeks were used for the experiment. All mice were kept in an SPF environment. All mice were kept under specific pathogen-free conditions, nurtured in an environment with proper temperature and humidity, and provided with abundant water and nourishment (25 °C, optimal humidity typically at 50%, and a 12-hour dark/light cycle). The pharmacokinetic profile of formulations was assessed via intravenous route of drug administration via tail vein of SD Rats (6-week-old). SD Rats ($n = 3$) were anaesthetized with isoflurane in oxygen. Anaesthetized mice were administered 30 mg/kg of formulation of solution through the tail vein. Blood samples (approx. 200 μL) were collected via mice eye socket vein at different time intervals up to 6 days. Plasma was extracted from blood samples by centrifugation at 5000 rpm for 15 min at 4 °C. Samples were stored at −80 °C until further analysis. The concentration of the BSA and BSA-multiblock polymer conjugates in plasma was calculated using the Rat rudimental bovine serum albumin (BSA) check-up ELISA kit (CUSABIO). A pre-dose sample (0 h) was drawn before the injection of the test compounds as a control. The data were quantified to generate pharmacokinetic parameters by Phoenix software using a two-compartment model.

Biodistribution of BSA and BSA-multiblock polymer conjugates

Male BALB/c mice received an intravenous injection of each Cy5.5-labeled BSA-multiblock polymer conjugate at a Cy5.5-equivalent dosage of 10 μg/ml (200 μL) to evaluate the biodistribution ($n = 3$). Major organs (heart, liver, spleen, lung, and kidney) were harvested at selected time points. The distribution was observed using a near-infrared (NIR) imaging system (IVIS Lumina II imaging system, USA) at different time points. Thereafter, mice were killed, and major organs were obtained and then observed by the NIR imaging system.

Statistical analysis

All data were presented as means ± standard deviation. Number of biologically independent samples (n) was indicated in the figure legends. Statistical comparisons were performed using GraphPad Prism 9 software with appropriate methods as indicated in the figure legends.

Reporting summary

Further information on research design is available in the Nature Portfolio Reporting Summary linked to this article.

Data availability

All data are available from the corresponding author upon request. All data generated in this study are provided in the Supplementary Information/Source Data file. Source data are provided with this paper. The BSA structure (PDB id: 4F5S) used in this study for MD simulations can be found in the Protein Data Bank (PDB). Source data are provided with this paper.

References

1. Lu, H. et al. Recent advances in the development of protein–protein interactions modulators: mechanisms and clinical trials. *Sig. Transduct. Target. Ther.* **5**, 213 (2020).
2. Herrera Estrada, L. P. & Champion, J. A. Protein nanoparticles for therapeutic protein delivery. *Biomater. Sci.* **3**, 787–799 (2015).
3. Ebrahimi, S. B. & Samanta, D. Engineering protein-based therapeutics through structural and chemical design. *Nat. Commun.* **14**, 2411 (2023).
4. Leader, B., Baca, Q. J. & Golan, D. E. Protein therapeutics: a summary and pharmacological classification. *Nat. Rev. Drug Discov.* **7**, 21–39 (2008).
5. Serna, N. et al. Protein-based therapeutic killing for cancer therapies. *Trends Biotechnol.* **36**, 318–335 (2018).
6. Harris, J. M. & Chess, R. B. Effect of pegylation on pharmaceuticals. *Nat. Rev. Drug Discov.* **2**, 214–221 (2003).
7. Wright, T. A., Page, R. C. & Konkolewicz, D. Polymer conjugation of proteins as a synthetic post-translational modification to impact their stability and activity. *Polym. Chem.* **10**, 434–454 (2019).
8. Zakas, P. M. et al. Enhancing the pharmaceutical properties of protein drugs by ancestral sequence reconstruction. *Nat. Biotechnol.* **35**, 35–37 (2017).
9. Doering, C. B., Healey, J. F., Parker, E. T., Barrow, R. T. & Lollar, P. Identification of porcine coagulation factor VIII domains responsible for high level expression via enhanced secretion. *J. Biol. Chem.* **279**, 6546–6552 (2004).
10. Liu, Y. et al. Mechano-bioconjugation strategy empowering fusion protein therapeutics with aggregation resistance, prolonged circulation, and enhanced antitumor efficacy. *J. Am. Chem. Soc.* **144**, 18387–18396 (2022).
11. Qu, Z. et al. A single-domain green fluorescent protein catenane. *Nat. Commun.* **14**, 3480 (2023).
12. Hou, Y. & Lu, H. Protein PEPylation: a new paradigm of protein–polymer conjugation. *Bioconjug. Chem.* **30**, 1604–1616 (2019).
13. Shimoboji, T. et al. Photoresponsive polymer–enzyme switches. *Proc. Natl Acad. Sci. USA* **99**, 16592–16596 (2002).
14. Carmali, S., Murata, H., Matyjaszewski, K. & Russell, A. J. Tailoring site specificity of bioconjugation using step-wise atom-transfer radical polymerization on proteins. *Biomacromolecules* **19**, 4044–4051 (2018).
15. Cobo, I., Li, M., Sumerlin, B. S. & Perrier, S. Smart hybrid materials by conjugation of responsive polymers to biomacromolecules. *Nat. Mater.* **14**, 143–159 (2015).
16. Kim, C. H., Axup, J. Y. & Schultz, P. G. Protein conjugation with genetically encoded unnatural amino acids. *Curr. Opin. Chem. Biol.* **17**, 412–419 (2013).
17. Dehn, S., Castelletto, V., Hamley, I. W. & Perrier, S. Altering peptide fibrillization by polymer conjugation. *Biomacromolecules* **13**, 2739–2747 (2012).
18. Jones, M. W. et al. Direct peptide bioconjugation/PEGylation at tyrosine with linear and branched polymeric diazonium salts. *J. Am. Chem. Soc.* **134**, 7406–7413 (2012).

19. Finbloom, J. A., Han, K., Slack, C. C., Furst, A. L. & Francis, M. B. Cucurbit[6]uril-promoted click chemistry for protein modification. *J. Am. Chem. Soc.* **139**, 9691–9697 (2017).
20. Hou, Y., Yuan, J., Zhou, Y., Yu, J. & Lu, H. A concise approach to site-specific topological protein–poly(amino acid) conjugates enabled by in situ-generated functionalities. *J. Am. Chem. Soc.* **138**, 10995–11000 (2016).
21. Wang, W. et al. Discrete, Chiral polymer–insulin conjugates. *J. Am. Chem. Soc.* **144**, 23332–23339 (2022).
22. Tucker, B. S. et al. Role of polymer architecture on the activity of polymer–protein conjugates for the treatment of accelerated bone loss disorders. *Biomacromolecules* **16**, 2374–2381 (2015).
23. Zhang, D. et al. A highly efficient and specific "grafting to" route for stable protein-polymer conjugates based on Spy chemistry. *Polymer* **275**, 125916 (2023).
24. Zhang, H., Weingart, J., Gruzdys, V. & Sun, X.-L. Synthesis of an end-to-end protein–glycopolymer conjugate via bio-orthogonal chemistry. *ACS Macro Lett.* **5**, 73–77 (2016).
25. Wang, J.-S. & Matyjaszewski, K. Controlled/"living" radical polymerization. Atom transfer radical polymerization in the presence of transition-metal complexes. *J. Am. Chem. Soc.* **117**, 5614–5615 (1995).
26. Averick, S. et al. ATRP under biologically relevant conditions: grafting from a protein. *ACS Macro Lett.* **1**, 6–10 (2012).
27. Heredia, K. L. et al. In situ preparation of protein–"smart" polymer conjugates with retention of bioactivity. *J. Am. Chem. Soc.* **127**, 16955–16960 (2005).
28. Mayadunne, R. T. A., Jeffery, J., Moad, G. & Rizzardo, E. Living free radical polymerization with reversible addition–fragmentation chain transfer (RAFT polymerization): approaches to star polymers. *Macromolecules* **36**, 1505–1513 (2003).
29. Boyer, C. et al. Well-defined protein–polymer conjugates via in-situ RAFT polymerization. *J. Am. Chem. Soc.* **129**, 7145–7154 (2007).
30. De, P., Li, M., Gondi, S. R. & Sumerlin, B. S. Temperature-regulated activity of responsive polymer–protein conjugates prepared by grafting-from via RAFT polymerization. *J. Am. Chem. Soc.* **130**, 11288–11289 (2008).
31. Lewis, A. L. *"Polymer conjugates." U.S. Patent No. 8,431,113*. U.S. Patent No. 8,431,113. (U.S. Patent and TrademarkOffice, 2013).
32. Lewis, A. L. & Leppard, S. W. "Conjugation reactions." U.S. Patent No.8,053,520. U.S. Patent No. 8,053,520. (U.S. Patent and Trademark Office, 2011).
33. Bhalchandra, S., Murata, L. H., Matyjaszewski, K. & Russell, A. J. Synthesis of uniform protein–polymer conjugates. *Biomacromolecules* **6**, 3380–3387 (2005).
34. Zhang, L. et al. Hypoxia-triggered bioreduction of poly(N-oxide)–drug conjugates enhances tumor penetration and antitumor efficacy. *J. Am. Chem. Soc.* **145**, 1707–1713 (2023).
35. Tucker, B. S., Coughlin, M. L., Figg, C. A. & Sumerlin, B. S. Grafting-from proteins using metal-free PET–RAFT polymerizations under mild visible-light irradiation. *ACS Macro Lett.* **6**, 452–457 (2017).
36. Theodorou, A. et al. Protein-polymer bioconjugates via a versatile oxygen tolerant photoinduced controlled radical polymerization approach. *Nat. Commun.* **11**, 1486 (2020).
37. Mansfield, K. M. & Maynard, H. D. Site-specific insulin-trehalose glycopolymer conjugate by grafting-from strategy improves bioactivity. *ACS Macro Lett.* **7**, 324–329 (2018).
38. Fu, C. et al. Low-fouling fluoropolymers for bioconjugation and in vivo tracking. *Angew. Chem. Int. Ed.* **59**, 4729–4735 (2020).
39. Lu, J., Wang, H., Tian, Z., Hou, Y. & Lu, H. Cryopolymerization of 1,2-dithiolanes for the facile and reversible grafting-from synthesis of protein–polydisulfide conjugates. *J. Am. Chem. Soc.* **142**, 1217–1221 (2020).
40. Gao, W., Liu, W., Christensen, T., Zalutsky, M. R. & Chilkoti, A. In situ growth of a PEG-like polymer from the C terminus of an intein fusion protein improves pharmacokinetics and tumor accumulation. *Proc. Natl Acad. Sci. USA* **107**, 16432–16437 (2010).
41. Pelegri-O'Day, E. M. & Maynard, H. D. Controlled radical polymerization as an enabling approach for the next generation of protein–polymer conjugates. *Acc. Chem. Res.* **49**, 1777–1785 (2016).
42. Wang, Y. & Wu, C. Site-specific conjugation of polymers to proteins. *Biomacromolecules* **19**, 1804–1825 (2018).
43. Zhang, Q. et al. Well-defined protein/peptide–polymer conjugates by aqueous Cu-LRP: synthesis and controlled self-sssembly. *J. Am. Chem. Soc.* **137**, 9344–9353 (2015).
44. Alexis, T. et al. Rapid oxygen-tolerant synthesis of protein-polymer bioconjugates via aqueous copper mediate polymerization. *Biomacromolecule* **23**, 4241–4253 (2022).
45. Lutz, J.-F., Ouchi, M., Liu, D. R. & Sawamoto, M. Sequence-controlled polymers. *Science* **341**, 1238149 (2013).
46. Badi, N. & Lutz, J.-F. Sequence control in polymer synthesis. *Chem. Soc. Rev.* **38**, 3383–3390 (2009).
47. DeStefano, A. J., Segalman, R. A. & Davidson, E. C. Where biology and traditional polymers meet: the potential of associating sequence-defined polymers for materials science. *JACS Au* **1**, 1556–1571 (2021).
48. Bates, F. S. et al. Multiblock polymers: panacea or pandora's box? *Science* **336**, 434–440 (2012).
49. Lutz, J.-F. Coding macromolecules: inputting information in polymers using monomer-based alphabets. *Macromolecules* **48**, 4759–4767 (2015).
50. Zhang, Q. et al. Sequence-controlled multi-block glycopolymers to inhibit DC-SIGN-gp120 binding. *Angew. Chem. Int. Ed.* **52**, 4435–4439 (2013).
51. Nikolaos, G. E. et al. Sequence-controlled methacrylic multiblock copolymers via sulfur-free RAFT emulsion polymerization. *Nat. Chem.* **9**, 171–178 (2017).
52. Dong, R. et al. Sequence-defined multifunctional polyethers via liquid-phase synthesis with molecular sieving. *Nat. Chem.* **11**, 136–145 (2019).
53. Shi, Q. et al. Digital micelles of encoded polymeric amphiphiles for direct sequence reading and ex vivo label-free quantification. *Nat. Chem.* **15**, 257–270 (2023).
54. Yu, L. et al. Digital synthetic polymers for information storage. *Chem. Soc. Rev.* **52**, 1529–1548 (2023).
55. Janatova, J., Fuller, J. K. & Hunter, M. J. The heterogeneity of bovine albumin with respect to sulfhydryl and dimer content. *J. Biol. Chem.* **243**, 3612–3622 (1968).
56. Le Droumaguet, B. & Velonia, K. In situ ATRP-mediated hierarchical formation of giant amphiphile bionanoreactors. *Angew. Chem. Int. Ed.* **47**, 6263–6266 (2008).
57. Lockridge, O. et al. Pseudo-esterase activity of human albumin: slow turnover on tryosine 411 and stabke acetylation of 82 residues including 59 lysines. *J. Biol. Chem.* **283**, 22582–22590 (2008).
58. Martínez, L., Andrade, R., Birgin, E. G. & Martínez, J. M. PACKMOL: a package for building initial configurations for molecular dynamics simulations. *J. Comput. Chem.* **30**, 2157–2164 (2009).
59. Valdés-Tresanco, M. S., Valdés-Tresanco, M. E., Valiente, P. A. & Moreno, E. gmx_MMPBSA: a new tool to perform end-state free energy calculations with GROMACS. *J. Chem. Theory Comput.* **17**, 6281–6291 (2021).

Acknowledgements

This work was financially supported by the National Natural Science Foundation of China (22175114 R.D., 22375124 R.D. and 22177072 L.D.), the Natural Science Foundation of Shanghai (22ZR1429400 R.D.), the National Science Fund for Excellent Young Scholars (Overseas)

(23Z990202541 R.D.), the High-Level Overseas Talents Introduction Program of Shanghai, the Research Startup Foundation of Shanghai Jiao Tong University, and the International Postdoctoral Exchange Fellowship Program (YJ20210136 L.Y.). We gratefully acknowledge the computational support from Xiaogan 3D Scientific Computing Center, where the extreme arithmetic power greatly reduces the computational time.

Author contributions

R.D. conceived and supervised this project. R.D. and Z.L. designed the experiments. Z.L. synthesized and characterized the materials. Z.L. and Y.S. conducted in vitro test. Z.L., Y.C., L.Y.(You), L.Y.(Yu), B.C., Q.H., Z.Y., and Y.X. carried out the animal test. K.S. and L.D. performed the MD simulations. Z.L., R.D., and X.Z. performed the date analyses. Z.L. and R.D. wrote the manuscript. R.D. revised the manuscript. All the authors contributed to the discussion and revision of the content, and agreed to the final version of the manuscript.

Competing interests

The authors declare no competing interests.

Additional information

Supplementary information The online version contains supplementary material available at https://doi.org/10.1038/s41467-024-51122-1.

Correspondence and requests for materials should be addressed to Lintai Da or Ruijiao Dong.

Peer review information *Nature Communications* thanks the anonymous reviewers for their contribution to the peer review of this work. A peer review file is available.